AMS Home   Journals Home   Journal Archive   Subscribe   For Authors   Help   Advanced Search   [Search]   Go

Full Text View

Orthobaric Density: A Thermodynamic Variable for Ocean Circulation Studies

Roland A. de Szoeke, Scott R. Springer, and David M. Oxilia

College of Oceanic and Atmospheric Sciences, Oregon State University, Corvallis, Oregon

ABSTRACT

A new density variable, empirically corrected for pressure, is constructed. This is done by first fitting compressibility (or sound speed) computed from global ocean datasets to an empirical function of pressure and in situ density (or specific volume). Then, by replacing true compressibility by this best-fit virtual compressibility in the thermodynamic density equation, an exact integral of a Pfaffian differential form can be found; this is called orthobaric density. The compressibility anomaly (true minus best-fit) is not neglected, but used to develop a gain factor ψ on the irreversible processes that contribute to the density equation and drive diapycnal motion. The complement of the gain factor, $\psi - 1$, multiplies the reversible motion of orthobaric density surfaces to make a second contribution to diapycnal motion. The gain factor is a diagnostic of the materiality of orthobaric density: gain factors of 1 would indicate that orthobaric density surfaces are as material as potential density surfaces. Calculations of the gain factor for extensive north–south ocean sections in the Atlantic and Pacific show that it generally lies between 0.8 and 1.2.

Orthobaric density in the ocean possesses advantages over potential density that commend its use as a vertical coordinate for both descriptive and modeling purposes. A geostrophic streamfunction exists for the momentum equations transformed to orthobaric density coordinates so that the gradients of orthobaric density surfaces give precisely the geostrophic shear. A form of Ertel's potential vorticity can be defined whose evolution equation contains no contribution from the baroclinicity vector. Orthobaric density surfaces are invariant to the choice of reference pressure. All of these are properties that potential density lacks.

In the continuous limit, patched potential density surfaces, which are formed by joining segments of locally referenced potential density surfaces in various pressure ranges and are extensively used in descriptive physical oceanography, become a particular form of orthobaric density surfaces. The method of selecting the segments is

Options:
- Create Reference
- Email this Article
- Add to MyArchive
- Search AMS Glossary

Search CrossRef for:
- Articles Citing This Article

Search Google Scholar for:
- Roland A. de Szoeke
- Scott R. Springer
- David M. Oxilia

equivalent to choosing the virtual compressibility function. This correspondence is a useful aid in interpreting patched potential density surfaces. In particular, there is a material flow across such surfaces that is analogous to the reversible flow across orthobaric isopycnals.

1. Introduction

In a companion paper (de Szoeke 2000) the equations of motion were set down in a form in which an arbitrary thermodynamical variable was used as vertical coordinate instead of depth. The variable was expressed as a function of pressure, specific volume, and salinity[1]; the only restriction on it was that it be monotonic with respect to depth. It was shown that, in general, using such a variable as a coordinate introduces into the momentum equations terms explicitly involving salinity gradients, multiplied by a thermodynamic coefficient that is determined by the specification of the coordinate variable. As this coefficient is the chemical potential when entropy is used as coordinate, it is termed the chemical potential analogue. If conventional potential density is used as vertical coordinate, these salinity-gradient terms are by no means negligible in pressure ranges more than a few hundred decibars from the reference pressure.

Potential density of seawater was originally put forward as a generalization of the notion of potential temperature for a single-component fluid like dry air (Wüst 1933; Montgomery 1938). In the case of dry air, potential temperature possesses dual thermodynamic and dynamic properties that make it uniquely useful. It is an alias of entropy, so it can change only because of irreversible processes, such as molecular diffusion, turbulent mixing, diabatic heating, cabbeling, etc.; we may call such a variable quasi-conservative or quasi-material. It is also the sole determinant in the fluid of the buoyant force due to density variations. Potential density of seawater, on the other hand, though it may be quasi-conservative, is severely lacking in its dynamical properties. It may exhibit inversions even in regions where the ocean is stably stratified (Ekman 1934; Lynn and Reid 1968). It is not the sole determinant of buoyant force, for salinity gradients on potential density surfaces may still generate significant contributions to the momentum balance (de Szoeke 2000). This behavior is a consequence of the thermobaric character of seawater, namely, that the thermal expansion coefficient of seawater depends strongly on pressure (Ekman 1934; McDougall 1987a).

McDougall (1987b; also Jackett and McDougall 1997) introduced the notion of neutral density to overcome some of the difficulties associated with potential density, including the problem of monotonicity when true stratification is stable. However, neutral density is not a thermodynamic function; it depends not only on the thermodynamic state of a water sample, characterized by the triplet of pressure, temperature, and salinity, but also on the geographical location where it was collected—a dependence determined by reference to a global hydrographic dataset. This hybrid character makes it difficult to work with, both theoretically and practically.

In this paper we shall consider thermodynamic variables that are *pycnotropic*—functions of pressure, p, and specific volume, α, only. Such a variable, when used as vertical coordinate, produces no extra gradient terms, besides the Montgomery function gradient, in the momentum balance equations (de Szoeke 2000). This pycnotropic property is what commends such variables for use in defining Ertel's (1942) potential vorticity. However, in general, pycnotropic variables lack the quasi-conservative property that potential density possesses: that the variable changes only because of irreversible processes that transport or create heat and salt.

The aim of this paper is to construct a variable, v, which we call empirical orthobaric specific volume, that is a function of p and α, monotonic in depth, and approximately quasi-conservative. By "approximate," we shall mean that adiabatic changes in v due to compressibility are as small as can be arranged for such a variable. We shall construct this variable by empirically fitting adiabatic compressibility (or sound speed) to a function of p and α, and then using this best-fit compressibility to construct an integral of the Pfaffian differential form for density.

The significance of orthobaric specific volume (or its reciprocal, orthobaric density) is twofold. It may be used as an alternative to potential density, conventional or patched, for purposes of descriptive display of oceanographic data. Because of its attractive dynamical and thermodynamic properties, it may be useful for theoretical manipulations and for numerical modeling of ocean circulation. Its dual usefulness for description and modeling derives from the same attributes.

The relation of orthobaric density surfaces to patched potential density surfaces, the latter constructed by joining segments of locally referenced potential density surfaces (Reid and Lynn 1971), will be examined (section 4). An interesting result will be established; namely, that in the limit of arbitrarily closely spaced locally referenced potential density segments, a form of orthobaric density is obtained. The specification of the matching of potential densities at the interfaces between their pressure ranges is equivalent to selecting the "best-fit," or virtual, compressibility. Just as regionally differentiated methods of patching potential density are employed (Reid 1994), geographically variable extensions of the orthobaric density idea may likewise be contemplated. The properties of the latter may be used to gain insight into the former.

2. Toward a quasi-conservative thermodynamic variable

A principal aim of this paper is to determine a variable

$$v = v(p, \alpha), \qquad (2.1)$$

a function only of pressure p and specific volume $\alpha = \rho^{-1}$, that is nearly quasi-conservative[2]; that is, its surfaces are nearly normal to the dianeutral vector. We start from the density equation, averaged over small-scale processes,

$$\frac{D\rho}{Dt} - \Gamma_\rho \frac{Dp}{Dt} = q. \qquad (2.2)$$

Here q specifies the sources and sinks of density due to (i) irreversible molecular fluxes of heat and salt, which are usually negligible; (ii) rectification due to nonlinearities in the equation of state, which produce cabbeling and thermobaric effects; and (iii) small-scale turbulent eddy transport divergences (McDougall 1987a; McDougall and Garrett 1992; Davis 1994). The second term on the left represents the reversible adiabatic compression in which Γ_ρ is the coefficient of adiabatic compressibility,[3] and may be considered a function of p, α, S:

$$\Gamma_\rho = 1/c^2(p, \alpha, S), \qquad (2.3)$$

c being the speed of sound. Suppose we write

$$\Gamma_\rho = \Gamma_0 + \Delta\Gamma, \qquad (2.4a)$$

where

$$\Gamma_0 = \frac{1}{c_0^2(p, \alpha)}, \qquad (2.4b)$$

$$\Delta\Gamma = \frac{1}{c^2(p, \alpha, S)} - \frac{1}{c_0^2(p, \alpha)}, \qquad (2.4c)$$

and $c_0^2(p, \alpha)$ shall be suitably chosen. We call Γ_0 the virtual or best-fit compressibility. The goal is to choose c_0^2 to make the compressibility anomaly $\Delta\Gamma$ as small as practicable. This will be taken up in the following sections.

Equation (2.2) may be written

$$\frac{D\alpha}{Dt} + \frac{\alpha^2}{c_0^2}\frac{Dp}{Dt} = -\alpha^2\Delta\Gamma\frac{Dp}{Dt} - \alpha^2 q. \qquad (2.5)$$

The left side of this is an exact Pfaffian differential; it may be written $\Phi Dv/Dt$, where Φ (an integrating factor) and v are pycnotropic functions determined as follows (Sneddon 1957). Define the virtual specific volume $A(p'|p, \alpha)$ by solving

$$\frac{\partial A}{\partial p'} = \frac{-A^2}{c_0^2(p', A)} \qquad (2.6a)$$

subject to

$$A(p|p, \alpha) = \alpha. \qquad (2.6b)$$

This is the potential specific volume relative to reference pressure p', obtained as though the adiabatic compressibility of seawater were $1/c_0^2(p, \alpha)$. At a fixed reference pressure, say $p' = 0$, $A(0|p, \alpha)$ defines a function

$$v(p, \alpha) = A(0|p, \alpha). \qquad (2.7)$$

We call v the orthobaric (meaning pressure-corrected) specific volume, conditioned on the choice of c_0.

The virtual specific volume may also be used to obtain the inverse function of (2.7), namely $\alpha(p, v)$. Replacing (2.6b) by

$$A(0|0, v) = v \qquad (2.6c)$$

and integrating (2.6a) to $p' = p$, the original in situ specific volume α must be recovered; namely,

$$\alpha(p, v) = A(p|0, v). \qquad (2.8)$$

A few members of this family, $\alpha = \alpha(p, v)$, for fixed v, that is, isopleths of v, are shown schematically on Fig. 1 ⬤. (Actual examples will be shown later, in Fig. 7 ⬤). The assignation of a numerical label v to the curves in Fig. 1 ⬤ corresponds to the specific volume that a hypothetical water parcel evolving according to (2.6a) would have at the reference pressure (zero in this case). Choosing a different reference pressure in (2.7) and (2.8) would alter the label of a particular curve in Fig. 1 ⬤ though not the form of the curve itself. The curves in Fig. 1 ⬤ are invariant in this sense, and selection of a reference pressure is arbitrary.

The integration factor ϕ is given by

$$\phi = \left(\frac{\partial \alpha}{\partial v}\right)_p. \qquad (2.9)$$

Because $\alpha(0, v) = A(0|0, v) = v$, it follows that $\phi = 1$ at $p = 0$. By differentiating Eq. (2.6a) for $\partial A(p'|0, v)/\partial p' = \partial \alpha(p', v)/\partial p'$ with respect to v, we may show that

$$\frac{\partial}{\partial p} \ln\phi = -\frac{\partial}{\partial \alpha}\left(\frac{\alpha^2}{c_0^2}\right). \qquad (2.10)$$

Given the well-behaved character of the right side of this equation, it is scarcely conceivable that ϕ can attain zero. Hence we conclude that $\phi > 0$ strictly.

De Szoeke (2000) showed two extreme examples of forms of orthobaric specific volume, conditioned respectively on the choices $c_0 = \infty$ and $c_0 = 0$. The former corresponds to in situ specific volume itself, while the latter can be thought of as pressure. While neither of these is particularly conservative, either may serve as a useful coordinate, especially pressure.

a. Standard salinity; compressibility anomaly

The virtual compressibility (2.4b) can be taken to define a standard salinity function $\overline{S}(p, \alpha)$ by means of the implicit relation

$$\Gamma_\rho(p, \alpha, \overline{S}(p, \alpha)) = \Gamma_0(p, \alpha). \qquad (2.11)$$

Hence the compressibility anomaly (2.4c) is

$$\Delta\Gamma = \Gamma_\rho(p, \alpha, S) - \Gamma_\rho[p, \alpha, \overline{S}(p, \alpha)]$$

$$\cong \left(\frac{\partial \Gamma_\rho}{\partial S}\right)_{p,\alpha} [S - \overline{S}(p, \alpha)]. \qquad (2.12)$$

Since $\Gamma_\rho = -\alpha^{-2}\partial\alpha/\partial p$, with θ, S held constant, a change of independent variables shows that

$$\left(\frac{\partial \Gamma_\rho}{\partial S}\right)_{p,\alpha} = \left(\frac{\partial \Gamma_\rho}{\partial S}\right)_{p,\theta} - \frac{\alpha_S}{\alpha_\theta}\left(\frac{\partial \Gamma_\rho}{\partial \theta}\right)_{p,S} = \alpha^{-2}\alpha_S \frac{\partial}{\partial p} \ln\left(\frac{\alpha_\theta}{\alpha_S}\right).$$

(2.13)

The expression after the first equality of (2.13) is strongly dominated by the second term. The expression after the second equality is proportional to McDougall's (1987a) thermobaric parameter T_b. It is also inversely proportional to the pressure (or depth) scale H_α displayed by Akitomo (1999; see that author's Fig. 1 ⊙):

$$\frac{\alpha^2}{\alpha_S}\left(\frac{\partial \Gamma_\rho}{\partial S}\right)_{p,\alpha} = \frac{\partial}{\partial p} \ln\left(\frac{\alpha_\theta}{-\alpha_S}\right) \equiv \frac{\alpha}{\alpha_\theta} T_b \cong \frac{\partial}{\partial p} \ln\alpha_\theta$$

$$\equiv H_\alpha^{-1}.$$

(2.14)

This shows that compressibility anomalies occur because of deviations of water mass properties, specifically of salinity from the standard salinity $\overline{S}(p, \alpha)$, coupled with the thermobaric character of seawater ($T_b \neq 0$).

b. Buoyancy frequency

The average buoyancy frequency n is defined by

$$n^2 = \frac{g}{\alpha}\frac{\partial \alpha}{\partial z} - \frac{g^2}{c^2},$$

(2.15)

and is calculated from the microstructure-averaged specific volume profile and the average compressibility (2.3). By using the hydrostatic relation,

$$\frac{\partial p}{\partial z} = \frac{p_\nu}{z_\nu} = -g\alpha^{-1},$$

(2.16)

one may write (2.15) as

$$n^2 = \frac{g}{\alpha}\left(\frac{\partial \alpha}{\partial z} + \frac{\alpha^2}{c_0^2}\frac{\partial p}{\partial z}\right) + \frac{g^2}{c_0^2} - \frac{g^2}{c^2},$$

the first term of which, multiplied by $\alpha g^{-1}\phi^{-1}$, is the exact differential $\partial \nu/\partial z$. Hence, using the second equality of (2.16), and (2.4c)

$$n^2 = -\frac{\phi g^2}{\alpha^2 p_\nu} - g^2\Delta\Gamma.$$

(2.17)

c. Gain factor

Equation (2.5) may be written

$$\dot{\nu} \equiv \frac{D\nu}{Dt} = -\phi^{-1}\alpha^2\Delta\Gamma\frac{Dp}{Dt} - \phi^{-1}\alpha^2 q. \quad (2.18)$$

The substantial derivative of pressure, written in terms of ν as independent variable, anticipating a result to be established below [Eq. (2.29)], is

$$\frac{D}{Dt}$$

where ∇_I is the gradient operator on surfaces of constant v. So Eq. (2.18) becomes

$$p_v \dot{\nu} = -p_v \psi \phi^{-1} \alpha^2 q + (\psi - 1)(\partial_t + \mathbf{u} \cdot \nabla_I)p, \tag{2.20}$$

where

$$\psi = (1 + \phi^{-1} \Delta \Gamma \alpha^2 p_v)^{-1}, \tag{2.21}$$

which will be called the buoyancy gain factor associated with v. This may be written, using (2.17),

$$\psi = \frac{\phi g}{\alpha n^2 z_v} = \frac{\phi g^2}{-\alpha^2 p_v n^2}, \tag{2.22}$$

or, upon eliminating p_v between (2.17) and (2.22),

$$\psi = 1 + \frac{g^2 \Delta \Gamma}{n^2} \tag{2.23}$$

[cf. McDougall (1989)].

In remarks following Eq. (2.10) we concluded that $\phi > 0$. Hence the condition for the validity of the transformation to v as vertical coordinate, namely that

$$\nu_z = 1/z_v > 0, \tag{2.24}$$

requires, from (2.22), that

$$\psi > 0. \tag{2.25}$$

(Actually, either sign of ψ is acceptable; only a change of sign is intolerable. By convention, we settle on the positive sign.)

The gain factor ψ is an index of the quasi-conservativeness of the scalar v. The irreversible sources and sinks of density (including small-scale turbulent diffusion), q, are multiplied by ψ to give the sinks and sources of v in Eq. (2.20). The other contribution to $\dot{\nu}$, containing the factor $(\psi - 1)$, is due to a remnant of the reversible compressibility effect. Large ψ is an indication of predominating reversible contributions to $\dot{\nu}$. [For example, if v were in situ specific volume, ψ could be $O(10)$ (de Szoeke 2000).] A choice of c_0^2 that renders ψ close to 1 will be sought.

d. The transformed equations of motion

The averaged primitive equations of motion can be put into a form that uses as vertical coordinate the orthobaric specific volume variable v described above by Eq. (2.7), provided only that condition (2.24) or (2.25) is met. These equations are

$$\frac{\partial}{\partial t}p_\nu + \nabla_I \cdot (p_\nu \mathbf{u}) + \frac{\partial}{\partial \nu}(p_\nu \dot{\nu}) = 0; \qquad (2.28)$$

where $\nabla_I \equiv (\partial_x, \partial_y)_\nu$ is the gradient operator along ν-isopleths, $\mathbf{u} = (u, \upsilon, 0)$, and $\mathbf{F}$ is the horizontal frictional force. Equation (2.20) should be substituted for $p_\nu \dot{\nu}$ in (2.28). The substantial rate of change operator is defined by

$$D/Dt \equiv \partial_t|_\nu + \mathbf{u} \cdot \nabla_I + \dot{\nu}\partial_\nu; \qquad (2.29)$$

the special functions appearing in (2.26)–(2.28) are

$$H = \int_0^p \alpha(p', \nu)\, dp', \qquad (2.30)$$

$$\Pi = \int_0^p \frac{\partial \alpha(p', \nu)}{\partial \nu}\, dp' \quad \text{(Exner function)}, \qquad (2.31)$$

$$M = H + gz \qquad \text{(Montgomery function).} \quad (2.32)$$

Details may be found in de Szoeke (2000). Notice particularly the absence of $\mu \nabla_I S$, $\mu \partial S/\partial \nu$ terms from (2.26) and (2.27). This is a consequence of the pycnotropic character of ν. Because of this also, an Ertelian potential vorticity can be defined,

$$Q = \frac{f + (v_x - u_y)|_\nu}{p_\nu}, \qquad (2.33)$$

which would be conserved if ν were conservative ($\dot{\nu} \equiv D\nu/Dt = 0$) and if friction were negligible ($\mathbf{F} = 0$). The function α (p, ν) to be used in (2.30), (2.31) is defined by Eq. (2.8); it is the inverse function of (2.7). From (2.9) and (2.31), the integrating factor ϕ is related to Π by

$$\phi = \left(\frac{\partial \Pi}{\partial p}\right)_\nu. \qquad (2.34)$$

Making the geostrophic approximation in (2.26), and using the hydrostatic balance (2.27), one may eliminate M from these equations to obtain the thermal wind balance,

$$f\mathbf{k} \times \partial_\nu \mathbf{u} = -\nabla_I \Pi. \qquad (2.35)$$

Hence gradients of the Exner function on orthobaric specific volume surfaces give the geostrophic "shear," $\partial_\nu \mathbf{u}$. On account of (2.34),

$$\nabla_I \Pi = \phi \nabla_I p, \qquad (2.36)$$

in which $\nabla_I p$ is practically the same as the slope of constant ν surfaces. There are no additional terms in (2.35), as there would be if the coordinate were potential density, for example (de Szoeke 2000).

e. Neutrality of orthobaric specific volume surfaces

Water parcels are often assumed to follow neutral trajectories that are everywhere perpendicular to the local dianeutral vector

$$\mathbf{e} = \nabla \alpha + \alpha^2 \Gamma_\rho \nabla p \qquad (2.37)$$

(McDougall 1987b; Davis 1994; Eden and Willebrand 1999). One may ask how closely neutral trajectories follow

orthobaric specific volume surfaces, $v = $ const, whose local normal is

$$\mathbf{e}_0 = \phi \nabla v = \nabla \alpha + \alpha^2 \Gamma_0 \nabla p. \qquad (2.38)$$

The angle β between $\mathbf{e}$ and $\mathbf{e}_0$ is given by

$$\sin \beta = \frac{|\mathbf{e}_0 \times \mathbf{e}|}{|\mathbf{e}_0||\mathbf{e}|}. \qquad (2.39)$$

Substituting, one obtains

$$\mathbf{e}_0 \times \mathbf{e} = \alpha^2 \Delta \Gamma \nabla \alpha \times \nabla p = \alpha^2 \Delta \Gamma \mathbf{e}_0 \times \nabla p$$
$$= \alpha^2 \Delta \Gamma \mathbf{e} \times \nabla p. \qquad (2.40)$$

Both $\mathbf{e}$ and $\mathbf{e}_0$ are dominated by their vertical components, so that (2.15) and (2.22) show that

$$|\mathbf{e}| \cong \frac{\alpha}{g} n^2, \qquad |\mathbf{e}_0| \cong \psi \frac{\alpha}{g} n^2. \qquad (2.41)$$

These are adequate approximations for the denominator of (2.39). Hence, using the second equality of (2.40), and (2.23),

$$\sin \beta \cong \left| (\psi - 1) \frac{\mathbf{e}_0 \times \nabla p}{\psi n^2} \right|. \qquad (2.42)$$

Using the first equality of (2.38), and (2.22),

$$\frac{\mathbf{e}_0 \times \nabla p}{\psi n^2} = \frac{\alpha}{g} \frac{\nabla v \times \nabla p}{v_z}.$$

Transforming the horizontal partial derivatives into derivatives along constant-v surfaces, one obtains

$$\sin \beta \cong |\psi - 1| \frac{\alpha}{g} [p_x^2 (1 + z_y^2) + p_y^2 (1 + z_x^2) - 2 p_x p_y z_x z_y]^{1/2}.$$

Because $|\nabla_I z| \ll 1$, this is very well approximated by

$$\sin \beta \cong |\psi - 1| \frac{\alpha}{g} |\nabla_I p|, \qquad (2.43)$$

where $\nabla_I p$ is the gradient of pressure in constant-v surfaces. Applying ∇_I to (2.30) and (2.32) and substituting in (2.43),

$$\sin \beta \cong |\psi - 1||\nabla_I z - g^{-1} \nabla_I M|. \qquad (2.44)$$

In this expression, $\nabla_I z$ is the slope of orthobaric specific volume surfaces, which one may take to change by hundreds of meters through the oceans, while $g^{-1} \nabla_I M$ is the gradient of dynamic height, which varies on the order of meters at most. Hence, (2.44) may be approximated by

$$\beta \cong |\psi - 1||\nabla_I z|. \qquad (2.45)$$

This means that the slope of a neutral trajectory at a point differs from the slope of the orthobaric specific volume surface through the same point by a proportion $|\psi - 1|$.

If the diffusivity tensor for the concentration of a scalar is diagonal with respect to principal axes oriented to the dianeutral vector $\mathbf{e}$ at a point,

$$\mathbf{K} = \mathrm{diag}(K_H, K_H, K_D), \qquad (2.46)$$

then the rotated tensor, with respect to axes oriented to $\mathbf{e}_0$, is

$$\mathbf{K}' \cong K_H \begin{pmatrix} 1 & -\beta_1\beta_2 & \beta_1 \\ -\beta_1\beta_2 & 1 & \beta_2 \\ \beta_1 & \beta_2 & K_D/K_H + \beta^2 \end{pmatrix}, \qquad (2.47)$$

where $(\beta_1, \beta_2) = (\psi - 1)\nabla_{\!\tilde{I}}z$ (Redi 1982; de Szoeke and Bennett 1993). The size of the term $K_H\beta^2$ enhancing the "true" dianeutral diffusivity K_D in the third diagonal element is a matter of particular concern. It is worth stressing that the orientation of the principal axes of $\mathbf{K}$ in (2.46) is an assumption, however plausible.

3. Orthobaric specific volume: An empirical pycnotropic variable

In this section we calculate a mean estimate of $c_0(p, \alpha)$ from the global distribution of temperature and salinity in the ocean and use it to construct an empirical orthobaric specific volume variable. We examine its suitability as a coordinate for use in modeling the World Ocean and analyzing oceanographic data.

From the global degree-square averaged National Oceanographic Data Center (NODC) hydrographic dataset of T and S at standard depths (Boyer and Levitus 1994), pressure, specific volume, and sound speed were calculated at every point on a three-dimensional spatial grid. Sound speeds were sorted into $\delta p \times \delta\alpha$ bins. The size of the δp bins was dictated by the standard depths of the NODC data and ranged from 10 dbar near the surface to 500 dbar at depth; each $\delta\alpha$ bin was chozen to be 0.005×10^{-5} m^3 kg^{-1} (corresponding to $\delta\rho = 0.05$ kg m^{-3}). The average sound speed, standard deviation, and number of points within each bin are shown in Figs. 2 ⊙, 3 ⊙, and 4 ⊙, respectively. In each of these figures the abscissa is adjusted specific volume,

$$\alpha^* = \alpha + \gamma p, \qquad (3.1)$$

where $\gamma = 3.941 \times 10^{-9}$ m^3 kg^{-1} dbar^{-1}. This adjustment is done purely for convenience to reduce the range of specific volume caused by pressure dependence, permitting a finer scale for α^*.

The colored region in Fig. 4 ⊙ represents the population density of water in the world's oceans with respect to pressure and specific volume. This region is relatively narrow in the deep ocean, reflecting the fact that there is little variation of specific volume there. The range of specific volume at a given pressure increases shallower than 1000 dbar, and becomes relatively large shallower than 500 dbar. Most of the region is contiguous, except on the left-hand side of the figure. Although there is no explicit geographic information contained in the figure, some parts of it can be identified with specific ocean basins because of their distinctive pressure-specific volume relationships. The detached region at the left, for example, corresponds to the Mediterranean and Red Seas. Because of the unusual water properties of these seas, their physical isolation from the rest of the oceans, as well as the poor coverage of these regions in the NODC data, we have decided to exclude these waters from further consideration in this calculation. Examination of the number of points in each $\delta p \times \delta\alpha^*$ bin (Fig. 4 ⊙) shows that most of the middepth water falls along one of two branches within the domain. The left branch represents the relatively denser (at a given pressure) waters of the Atlantic Ocean, and the right branch represents the less dense waters of the Pacific Ocean.

The bin-averaged sound speed, c_0, has a fairly simple dependence on pressure and specific volume. Figure 2 ⊙ displays averaged adjusted sound speed

$$c_0^* = c_0 - \lambda p \qquad (3.2)$$

with $\lambda = 0.018$ m s^{-1} dbar^{-1}. The λ parameter is arbitrarily chosen to reduce the linear trend in the dependence of sound speed on pressure that would otherwise dominate the figure. Usually, at a given pressure, sound speed increases with increasing specific volume. This is expected, as both sound speed and specific volume increase with temperature. (An exception to this rule occurs on the far left-hand side of the domain where there are low specific volumes but high sound

speeds owing to the warm but very salty waters found in the Mediterranean and Red Seas.) The average adjusted sound speed c_0^* in Fig. 2 ⊙ may be considered an empirical function relating sound speed to pressure and adjusted specific volume α^*.

Standard deviation, shown in Fig. 3 ⊙, quantifies the variability of the true sound speed about the bin-averaged sound speed. It is generally smaller than 10 m s^{-1} except in the upper ocean at pressures less than 300 dbar, where it may exceed 40 m s^{-1}. In the mid and deep ocean at pressures greater than 1000 dbar (Fig. 3 ⊙ inset), the standard deviation is 8 m s^{-1} or smaller. Variability in the sound speed estimate comes from two sources. The first is the intrinsic error of projecting a function of three independent variables (p, α^*, S) onto a function of just two independent variables (p, α^*). The second is the discretization error, that arises from gridding the data in the first stage of our analysis. In addition, the NODC data themselves have been subject to considerable smoothing and binning, which may also affect the calculation.

To assess the possible effects of the analysis procedure, which is applied in producing the gridded data, we independently calculated an empirical sound speed function directly from hydrographic data available from WOCE cruises and other sources. The geographic distribution of these data are shown in Fig. 5 ⊙. Though extensive horizontal coverage is plainly lacking, the very high vertical resolution makes possible a much finer bin size in pressure (2 dbar). The difference between the WOCE-derived empirical sound speed function and the NODC function (Fig. 2 ⊙) is shown in Fig. 6 ⊙. In the areas of the p, α^* plane where the datasets overlap, the differences are small. They are less than 20 m s^{-1} within the top 500 dbar of the ocean, and less than 2 m s^{-1} deeper than 1000 dbar (Fig. 6 ⊙ inset). Since these differences are smaller than the standard deviation of the NODC data, we conclude that the preprocessing applied to the NODC data has not compromised it for this purpose.

Favoring the distributed horizontal coverage of the NODC data, we used the average adjusted sound speed function of Fig. 2 ⊙ to calculate orthobaric specific volume v. The adjusted specific volume is related to the virtual specific volume function of section 2 by Eqs. (2.8), (3.1),

$$\alpha^*(p, v) = A(p|0, v) + \gamma p. \qquad (3.3)$$

In terms of this, the differential equation (2.6a) becomes

$$\frac{\partial \alpha^*}{\partial p} = \gamma - \frac{(\alpha^* - \gamma p)^2}{[c_0^*(p, \alpha^*) + \lambda p]^2}, \qquad (3.4a)$$

subject to

$$\alpha^* = v \quad \text{at } p = 0. \qquad (3.4b)$$

A Runge–Kutta procedure was used to integrate Eq. (3.4a). The resulting trajectories are shown in Fig. 7 ⊙. They are contours of constant v, when the latter is thought of as a function of p and α^*. Such contours exist throughout the populous regions of the domain. Away from the sea surface, the value of v at a given pressure is greater than α^*, reflecting the effect of pressure on specific volume. (Recall that much of the linear effect of pressure has already been removed in the transformation to α^*; without the transformation, these contours would extend much farther to the left of Fig. 7 ⊙.) The contours of v also have curvature owing to the nonlinear dependence of compressibility on pressure. Furthermore, the contours of v diverge with increasing pressure because of the dependence of c_0^* on α^* on the right-hand side of Eq. (3.4a). The spacing of the contours at great pressure is more than twice that at zero pressure. This reflects the approximate doubling of Φ [Eqs. (2.9), (2.34)] between surface and great pressure—the origin of which lies in the thermobaric effect (McDougall 1987a; de Szoeke 2000).

Various fields relevant to the calculation of orthobaric specific volume are displayed for two north–south WOCE sections in the Pacific and Atlantic (Tsuchiya et al. 1992, 1994), nominally along 150°W and 25°W (Fig. 5 ⊙). Sound speed anomaly,

$$\Delta c = c_0 - c, \qquad (3.5)$$

between average sound speed function $c_0(p, \alpha)$ (Fig. 2 ⊙) and actual sound speed is shown in Fig. 8 ⊙. [The linear trend λp removed from c_0 by (3.2) has been restored.] Note that compressibility anomaly $\Delta\Gamma$, given by (2.4c), may be obtained from

$$\Delta\Gamma \simeq 2c_0^{-3}\Delta c \qquad (3.6)$$

to good approximation. Sound speed anomalies are large and negative in the upper North Atlantic, while $\Delta c \sim -15$ m s^{-1} for depths shallower than 1500 m. Anomalies are moderately large and positive in the upper South Atlantic, $\Delta c \sim 5$ m s^{-1} shallower than 1500 m, though with a lens of negative anomaly, $\Delta c \sim -5$ m s^{-1} shallower than 600 m, in the subtropical South Atlantic. In the deep Atlantic small negative anomalies are found, between 0 and -5 m s^{-1}, with somewhat larger magnitudes in the deep North Atlantic. Small positive values occur along the bottom associated with Antarctic waters. Sound speed anomaly is invariably associated with salinity (Fig. 9 ⊙): negative anomalies with high salinity anomalies, and vice versa.

Sound speed anomalies are generally smaller in magnitude in the Pacific, and mostly positive, while in the Atlantic they are mostly negative. This merely reflects the fresher waters of the Pacific (Fig. 9 ⊙). Values are large in the upper North Pacific, with Δc of order 10 m s^{-1} shallower than 1000 m, somewhat smaller in the South Pacific at the same depths, the largest values occurring in the Antarctic Circumpolar Current. The only negative values are found shallower than 500 m in the subtropical gyre of the South Pacific, and between 500 m and 1500 m in the tropical band.

Buoyancy frequency is shown in Fig. 10 ⊙. This resembles what is seen, for example, in Flatté's (1979) section of this variable. It is included here because of the role it plays in the calculation of the buoyancy gain factor ψ [Eq. (2.23)]. The 0.4 cph [$=7.0 \times 10^{-4}$ rad s^{-1}] contour is shown dashed. This value corresponds to a density gradient of 0.01 kg m^{-3}/200 m, the numerator corresponding to the limit of density difference that can be discriminated (Fofonoff 1985) over the 200-m resolution sought in Fig. 10 ⊙. Values smaller than this we take to be not practically distinguishable from zero.

The gain factor ψ associated with orthobaric density [Eq. (2.23)] is shown in Fig. 11 ⊙. This factor lies mostly in the range 0.8 to 1.2 throughout both oceans outside the bottom layer with buoyancy frequency <0.4 cph, with occasional bull's-eyes in the upper ocean, presumably associated with mixed layers. In the deep North Atlantic, ψ values as low as 0.6 are found on the section, but only at the very edge of the bottom pycnostad, where the estimate of n^2 that goes into the calculation of ψ is marginally reliable. Values of ψ tend to be smaller than 1 in the Atlantic, associated with more-saline water masses, except for the fresher Antarctic waters and their equatorward extensions—intermediate water and bottom water. By contrast, values tend to be larger than 1 in the Pacific because waters are fresher, except in the near-surface South Pacific subtropics and in a middepth equatorial band. In the Pacific, values of ψ are somewhat nearer 1 than in the Atlantic.

The gain factor ψ is an index of the quality of orthobaric specific volume v as a coordinate. It is necessary for the transformation to v that ψ remain the same sign everywhere—a requirement that is easily satisfied. The irreversible sources of in situ density q are multiplied by ψ to give the irreversible sources of v [Eq. (2.20)]. The closeness of this factor to 1 makes the correction practically inconsequential. The turbulent mixing coefficients and such, which constitute the calculation of q, are far more uncertain than order 20%.

The rate of change of pressure, calculated as though observed following orthobaric specific volume surfaces, and multiplied by $\psi - 1$, makes a thermodynamically reversible contribution to $\dot{v}$. Though the $\psi - 1$ factor may be small, of order ±0.1, the effect of this contribution should not be neglected. In the next section, we shall demonstrate a link between patched potential density (Reid and Lynn 1971) and a form of orthobaric density, and show that, through the rifts between the leaves constituting the patched surfaces, there is a material flow that is the discrete analog of the reversible contribution to $\dot{v}$.

Meridional sections of the index of neutrality β^2, calculated from Eq. (2.45), are displayed in Fig. 12 ⊙ on a logarithmic scale. The largest values, $\geq O(10^{-8})$, are found along the ocean bottom, almost invariably within the band where buoyancy frequency is less than 0.4 cph, and where the estimates of $\psi - 1$, hence β^2, are most uncertain. Outside this band β^2 is typically orders of magnitude smaller. The criterion for the neglect of the $K_H\beta^2$ term in the third diagonal element of $\mathbf{K}'$, the diffusivity tensor with respect to orthobaric density coordinates, Eq. (2.47), is that

$$\beta^2 \lesssim K_D/K_H \approx 10^{-8}. \qquad (3.7)$$

To estimate the right side of this inequality, we have adopted the nominal values $K_D = 10^{-5}$ m^2 s^{-1}, $K_H = 10^3$ m^2 s^{-1}. This criterion is fairly well satisfied throughout the sections of Fig. 12 ⊙. We conclude that for the purposes of calculating turbulent diffusion with respect to orthobaric density surfaces, that is, the term q appearing in (2.2) or (2.20), the

approximation of the diagonal elements of $\mathbf{K}'$ [Eq. (2.47)] as K_H, K_H, K_D is acceptable.

Finally, sections of orthobaric density, shown as

$$\sigma_\nu = \nu^{-1} - 1000, \qquad (3.8)$$

are displayed in Fig. 13 ⊙. These sections appear quite conventional, exhibiting the features expected in "density" sections. However, the use of orthobaric density has certain advantages over potential density. Surfaces of constant orthobaric density (called orthobaric isopycnals, for short) are invariant with respect to reference pressure. If the reference pressure of Eq. (3.4b) were altered, the forms of the orthobaric isopycnals in Fig. 13 ⊙ would not change, although the numerical labels, σ_ν, of the surfaces would. Potential temperature also has this reference-invariant property,[4] though potential density in seawater does not. Second, the gradients of orthobaric isopycnals in Fig. 13 ⊙ give precisely the geostrophic shear [Eq. (2.35)], which gradients of potential density surfaces do not (de Szoeke 2000).

The chief reservation about using orthobaric density for descriptive and modeling purposes is the occurrence of residual compressibility contributions to diapycnal material flow, though this is an irreducible concomitant of the variable composition of seawater and thermobaric effects. This contribution is measured by the parameter $\psi - 1$, a nondimensional formulation of the compressibility anomaly $\Delta\Gamma$. Orthobaric density sections like Fig. 13 ⊙ ought to be evaluated in conjunction with the corresponding sections of ψ like Fig. 11 ⊙, which we discussed extensively above. In the following section we will show that a similar contribution to diapycnal mass flow must occur through patched potential density surfaces.

Interested readers may obtain datasets of the empirical function $c_0^*(p, \alpha^*)$ from the authors. Using these, Eqs. (3.4) may be solved by standard methods to obtain trajectories of constant ν on the p, α^* plane. In addition, a Matlab toolbox is available to compute orthobaric density, σ_ν, from hydrographic data for arbitrarily dimensioned (p, S, T) arrays.

4. Patched potential density

To overcome some of the difficulties with the use of potential density in pressure ranges far from its reference pressure, Reid and Lynn (1971) calculated potential densities over restricted pressure ranges (typically of order 1000 dbar) referenced to a pressure in the center of the range. We shall call a constant potential density surface within such a restricted pressure range a *leaf*. Patched isopycnal "surfaces" are formed by joining adjacent leaves across the transitions between their pressure ranges (Fig. 14a ⊙). The word "surfaces" is put in quotes here because of the inevitable discordances between the leaves, which must occur at their joints and which arise from the variation of compressibility with temperature (the thermobaric effect) and the geographical variation of T–S properties.

In this section we shall study the Reid and Lynn (1971) method of patching potential density leaves. In particular, we shall examine the discordances between the leaves, showing how they permit exchange of water through the resulting patched surfaces, even if the individual leaves are considered impermeable (i.e., when no mixing or cabbeling is held to occur across potential density surfaces), and calculate the rate of exchange across the discordances. It will be shown that patched potential density surfaces tend, in the limit of ever finer individual leaves (finer divisions of pressure intervals), to constant surfaces of a form of orthobaric density. This means that the procedure of matching leaves at the joints, as described above, is equivalent to replacement of true seawater compressibility by an approximate form, dependent only on pressure and specific volume, just as was done to obtain the empirical orthobaric density of sections 2 and 3. The rate of mass exchange across the discordances between leaves is the discrete analog of the reversible flux, obtained above, of water across the corresponding form of orthobaric density surfaces.

Potential density patching as it is usually practiced allows for regional variation of the patching procedure. For example, Reid (1994) patches the $\sigma_1 = 31.938$ leaf to the $\sigma_0 = 27.44$ leaf in the North Atlantic and to the $\sigma_0 = 27.30$ leaf in the South Atlantic. This is done to allow for regional differences in the T–S property distributions of the two oceans. We shall see in this situation that, while mass exchange through the discordances may be reduced in the individual subregions, additional horizontal mass exchanges through the patched potential density surfaces may arise at the discontinuous horizontal joints between the subregions. However, to begin, we shall put aside for later this complication of regionally differentiated patching and assume that a given σ_1 leaf, for example, is uniquely associated with a single σ_0 leaf everywhere. We may call this a universal form of patched potential density.

a. Patched isopycnals: A formal description

We show in Table 1 ⊙ excerpts of similar tables from Reid's (1994) analysis of circulation in the North and South

Atlantic. The rows in Table 1 ⊙ identify the $\sigma_m = a^{-1}{}_m - 1000$ values, with respect to reference pressures p_m, for $m = 0$, 1, 2, 3, 4, of certain potential density leaves defined, respectively, over the ranges $\overline{P}_m < p < \overline{P}_{m+1}$ [where $\overline{S}_m = \frac{1}{2}(p_m + p_{m-1})$ for $m > 0$, and $\overline{P}_0 = 0$]. The concatenation of these leaves from each row in Table 1 ⊙ gives a patched potential density surface [called simply an isopycnal surface by Reid and Lynn (1971), though we shall call it a patched isopycnal surface, to distinguish it from other kinds of isopycnal surfaces]. For example, in the North Atlantic, a leaf with density of 27.44 between the surface and 500 dbar is connected to the $\sigma_1 = 31.938$ leaf from 500 to 1500 dbar, and so on (Fig. 14a ⊙). It is convenient to label such a patched isopycnal surface by the numerical value of its σ_4 leaf. Reid (1994) follows this same practice, except when a surface never extends to greater than 3500 dbar, in which case the σ_m value of its deepest occurring leaf is used (Table 1 ⊙). We will not follow in this exception but always use a σ_4 label, obtained by extrapolation if necessary. This extrapolation is arbitrary but of no consequence except in furnishing a unique σ_4 label for each surface.

The entries from Table 1 ⊙ (denoted by pluses) have been plotted on Fig. 15 ⊙ as

$$\alpha^* = (\sigma_m + 1000)^{-1} + \gamma p \qquad (4.1)$$

[cf. Eq. (3.1)] versus σ_N (specifically σ_4, i.e., $N = 4$), and joined by straight lines for each reference pressure $p_m = 0$, 1, 2, 3, 4 hbar (1 hbar = 1000 dbar). The curves in Fig. 15 ⊙ may be read as defining a relation between σ_N and σ_m

$$\sigma_m = \hat{\sigma}(p_m, \sigma_N) \qquad (4.2)$$

at the discrete pressures p_m. Given any in situ density and pressure, σ_m and p_m, one can identify the corresponding reference pressure level and look up the corresponding isopycnal value (σ_4 in the case of Fig. 15 ⊙). [Note that trivially $\hat{\sigma}(p_N, \sigma_N) = \sigma_N$.] The function (4.2) furnishes the chain of σ_m values whose leaves make up a patched potential density surface characterized by the density label σ_N.

Suppose a water sample from pressure p_m, with (in situ) density $\sigma_m = \hat{\sigma}(p_m, \sigma_N)$ and salinity S, is taken adiabatically and with fixed composition to pressure p_{m+1}. There it will have a density $\sigma_{\text{pot}}(p_{m+1}|p_m, \sigma_m, S)$, where the function $\sigma_{\text{pot}}(p'|p, \sigma, S)$ gives the potential density, with respect to reference pressure p', of a water sample with in situ pressure p, density σ, and salinity S. This density matches $\sigma_{m+1} = \hat{\sigma}(p_{m+1}, \sigma_N)$ only for a special value of salinity given by the solution of

$$\sigma_{\text{pot}}(p_{m+1}|p_m, \sigma_m, \overline{S}) = \hat{\sigma}(p_{m+1}, \sigma_N). \qquad (4.3)$$

This special salinity value is designated by

$$\overline{S} = \overline{S}(p_m, p_{m+1}, \sigma_m), \qquad (4.4)$$

indicating its dependence on the pressure levels p_m, p_{m+1} and on the density value σ_m of the upper isopycnal surface. [The dependence on σ_N can be eliminated by inverting (4.2); listing the dependence on σ_{m+1} would be similarly superfluous.] If this value of salinity occurs at a point along the intersection of the $\sigma_m = \hat{\sigma}(p_m, \sigma_N) = \text{const}$ leaf with the transition pressure level $\overline{P}_{m+1}$, then the $\sigma_{m+1} = \hat{\sigma}(p_{m+1}, \sigma_N) = \text{const}$ leaf will pass through the same point. (Figure 14a ⊙ furnishes a schematic illustration of such an occurrence between a σ_0 surface and a σ_1 surface at 500 dbar.)

The Reid and Lynn (1971) method for selecting the set $\{\sigma_m\}$ of density leaves that constitute a patched isopycnal surface is illustrated in the θ–S diagram of Fig. 14b ⊙ for $m = 0$, that is, at the transition from σ_0 to σ_1 at the $\overline{P}_0 = 500$ dbar pressure level. The σ_1 surface to be associated with σ_0 is chosen to pass centrally through the range of the observed data points. (The details of this selection procedure need not concern us.) The important point is that there is a finite, even if narrow, range of observed θ, S values along any σ_0 surface at 500 dbar (say). This range differs from the θ, S values along the σ_1 surface chosen to correspond. This means that in physical space, illustrated schematically in Fig. 14a ⊙, the σ_0 leaf

intersecting 500 dbar cannot join perfectly onto the corresponding σ_1 leaf. The intersection of the chosen σ_0, σ_1 surfaces in the θ–S diagram of Fig. 14b ⊙ defines the salinity value $\overline{S}(0, 1000 \text{ dbar}, \sigma_0)$ used in Eq. (4.4) above. These methods readily generalize to give a value of σ_{m+1} corresponding to a preselected σ_m. In this way the set of leaves $\{\sigma_m : \overline{P}_m < p < \overline{P}_{m+1}\}$ that make up a patched surface may be constructed.

b. Coarse orthobaric density approximations to patched density

Before considering the theoretical limit of taking ever finer spacings of the set of reference pressures p_m, it is useful to review some interesting interpretations of the information in Table 1 ⊙ and Fig. 15 ⊙. The latter shows how coarsely resolved are the particular patched isopycnals displayed by Reid (1994): first, the pressure intervals over which the constituent leaves are defined are quite wide; second, only a small number (nine)[5] of isopycnal patchings are specified to represent the entire density continuum. (We will call these the standard patched isopycnals.)

On the second point, one might readily specify a continuum of intermediate patched isopycnals merely by linearly interpolating (for example) between the standard patched isopycnals. On the first point, the function $\hat{\sigma}(p_m, \sigma_4)$ gives the in situ densities, at the discrete pressures $p_m = 0, 1, 2, 3, 4$ hbar, that are associated with a given σ_4 label. Although the patched isopycnals appear to admit no interpretation of $\hat{\sigma}$ at pressures intermediate between these discrete values, each of which stands for a finite range, one might interpret an interpolation between these discrete pressures as follows. Consider two simple choices of interpolation indicated in Fig. 16 ⊙. This shows $\alpha^* = (\hat{\sigma} + 1000)^{-1} + \gamma p$, in situ specific volume corrected by the offset γp, as a function of p for $\sigma_4 = 45.88$. The discrete data points, denoted by asterisks, have been joined in two ways: by a sequence of centered stair steps and by linear segments. For either choice of interpolation (or any other) Fig. 16 ⊙ may be read as specifying the in situ density $\hat{\sigma}$ at pressure p that is to be associated with the given σ_4 label. Conversely, the numerical σ_4 label of a water parcel with in situ density $\hat{\sigma}$ at pressure p, converted to α^*, may be read off Fig. 15 ⊙, and identifies a surface of water parcels that share this label. This surface is an isopleth of a form of orthobaric density, whose value coincides with in situ density at 4 hbar. The two interpolation choices give two forms of orthobaric density. The stair-step orthobaric density isopleths correspond fairly closely to the potential density leaves, patched together at the transition pressures: within each pressure interval the in situ density, *after correction for pressure,* is constant.[6] Figure 16 ⊙ also shows the orthobaric density isopleth from Fig. 7 ⊙, based on globally averaged compressibility, that goes through $\hat{\sigma} = 45.88$ at $p = 4$ hbar. Error bars (± 2 std dev, encompassing 95% confidence) are shown on the global orthobaric isopycnal. These are computed by summing variance estimates of sound speed from the $\delta p \times \delta \alpha$ bins of Fig. 3 ⊙ from the starting point of integration of (2.6)—$p' = 4$ hbar—to pressure p, namely,

$$\text{var}_\alpha(p) = \sum_{p'=p}^{4 \text{ hb}} \left(\frac{2\alpha^2 \Delta p}{c_0^3}\right)^2 \text{var}_c(p'),$$

as though sound speed fluctuations were uncorrelated among bins. These error bars may be interpreted as defining an envelope likely to contain at 95% confidence the statistically expected orthobaric isopycnal based on the expectation value of the (p, α)-sorted sound speed. The linearly interpolated versions of Reid's (1994) patched isopycnals for the South and North Atlantic are quite close to the global-average orthobaric isopycnal, lying mostly within the error bars.

There is no fundamental reason to favor the stair-step interpolation over linear interpolation, each of which gives a different form of orthobaric density. Note that the virtual compressibility function, $\Gamma_0 = (\partial\hat{\sigma}/\partial p)_{\sigma_N}$, is infinite at the transition pressures for the stair-step orthobaric density, but remains finite for the linearly interpolated orthobaric density. A coarse version of Fig. 2 ⊙ could be constructed by differencing the rows of Table 1 ⊙.

c. Patched potential density: The continuous limit

We turn now to the question of taking the limit of ever finer spacing of the potential density leaves in patched surfaces, that is, taking each $\Delta p = p_{m+1} - p_m \to 0$. It will first be shown how the salinity function (4.4) generates a virtual compressibility function, which defines a kind of orthobaric density. Subtract $\sigma_m = \sigma_{pot}(p_m|p_m, \sigma_m, \overline{S}) = \hat{\sigma}(p_m, \sigma_N)$ from both sides of Eq. (4.3), where $\overline{S}$ is given by (4.4), and divide by Δp:

$$\frac{\sigma_{\text{pot}}(p_{m+1}|p_m, \sigma_m, \overline{S}) - \sigma_{\text{pot}}(p_m|p_m, \sigma_m, \overline{S})}{\Delta p}$$

$$= \frac{\hat{\sigma}(p_{m+1}, \sigma_N) - \hat{\sigma}(p_m, \sigma_N)}{\Delta p}. \tag{4.5}$$

In the limit $\Delta p \rightarrow 0$, the left side becomes

$$\left.\frac{\partial \sigma_{\text{pot}}(p'|p_m, \sigma_m, \overline{S})}{\partial p'}\right|_{p'=p_m} = \Gamma_\rho(p_m, \sigma_m, \overline{S}). \tag{4.6}$$

This is the partial rate of change of potential density with respect to reference pressure, and is therefore the adiabatic compressibility evaluated at p_m, σ_m, $\overline{S}(p_m, p_{m+1}, \sigma_m)$ ([Phillips 1966](#)). In the limit this may be written

$$\Gamma_\rho(p, \sigma, \overline{S}(p, \sigma)) \equiv \Gamma_0(p, \sigma), \tag{4.7}$$

where

$$\sigma = \hat{\sigma}(p, \sigma_N) \tag{4.8}$$

and

$$\overline{S}(p, \sigma) = \lim_{p_{m+1} \rightarrow p_m} \overline{S}(p_m, p_{m+1}, \sigma_m) \tag{4.9}$$

are the continuous limits of [(4.2)](#) and [(4.4)](#). (The subscripts m, superfluous in the limit, have been dropped.)

The right side of [(4.5)](#), in the limit $\Delta p \rightarrow 0$, becomes $\partial\hat{\sigma}(p', \sigma_N)/\partial p'$. Putting all this together, one sees that the function $\hat{\sigma}(p', \sigma_N)$ is given by the solution of the differential equation

$$\frac{\partial \hat{\sigma}}{\partial p'} = \Gamma_0(p', \hat{\sigma}), \tag{4.10a}$$

subject to

$$\hat{\sigma} = \sigma_N \text{ at } p' = p_N. \tag{4.10b}$$

[Equation (4.7)](#) defines a virtual compressibility function, Γ_0, dependent only on pressure, p, and in situ density, σ, and conditioned on $\overline{S}(p, \sigma)$, the continuous limit of [(4.4)](#). Comparison of [(4.7)](#) with [(2.11)](#) confirms that $\overline{S}(p, \sigma)$ is identical to the standard salinity function defined in [section 2](#). [Equation (4.8)](#) describes the in situ density at pressure p that is to be used in constructing the continuous limit of the patched isopycnal surface generated from the reference density σ_N. Comparing (4.10) to [Eqs. (2.6a,c)](#), [(2.8)](#) one sees, by making the identifications

$$\left.\begin{array}{l} \hat{\sigma} = \alpha^{-1} - 1000 \\ \sigma_N = \nu^{-1} - 1000 \\ \Gamma_0 = 1/c_0^2(p, \alpha) \end{array}\right\} \tag{4.11}$$

that the equations are identical.

d. Quasi-conservative property

In the discrete version of patched density, the potential densities of individual leaves are quasi-conservative. In the continuous limit a form of orthobaric density is recovered, which is not in general quasi-conservative, as we saw in section 2. This apparent paradox is resolved by observing that there is concentrated reversible material flow through the joints between the individual leaves of the patched isopycnals. This becomes continuously distributed in the limit and is synonymous with the reversible material flow, given by the second term of Eq. (2.20), across the limiting orthobaric isopycnals. The recognition of this material flow across patched surfaces (as across orthobaric isopycnals) is important to the assessment of the meaning of such surfaces in practical oceanographic contexts. For this reason we offer the following thought experiment that illustrates the inevitability of the cross-surface flow at the transitions between potential density leaves.

Suppose a subsurface ballasted float, which otherwise is advected by horizontal fluid motion, is programmed to adjust its buoyancy so as to follow patched potential density surfaces. Suppose the float is following a σ_m leaf in the downward sense and approaching the transition pressure $\overline{P}_{m+1}$ at which it will switch to follow a σ_{m+1} leaf. The particular σ_{m+1} leaf to which it will switch has the value $\hat{\sigma}(p_{m+1}, \sigma_N)$, preassigned by the Reid and Lynn (1971) procedure, and given by (4.3) at the salinity $\overline{S}$ specified by (4.4). Before the transition, the thermodynamic state of the water parcel surrounding the float is completely described by σ_m, p_m, and its *actual* salinity S. The potential density referenced to p_{m+1} of this water parcel is $\sigma_{pot}(p_{m+1}|p_m, \sigma_m, S)$. The difference of this value from the target potential density is therefore

$$\Delta\sigma = \sigma_{pot}(p_{m+1}|p_m, \sigma_m, S)$$
$$- \sigma_{pot}[p_{m+1}|p_m, \sigma_m, \overline{S}(p_m, p_{m+1}, \sigma_m)]. \quad (4.14)$$

By carrying out successive Taylor expansions, first of p_{m+1} about p_m at fixed S (or $\overline{S}$) and σ_m, then of S about $\overline{S}$, and using (4.6), one obtains that (4.14) is approximately

$$\Delta\sigma \cong \left(\frac{\partial\Gamma_\rho}{\partial S}\right)_{p,\alpha} [S - \overline{S}(p_m, p_{m+1}, \sigma_n)](p_{m+1} - p_m), \quad (4.15)$$

where the coefficient is furnished by (2.13). This is the in situ density change through which the float must instantaneously be made to rise or drop to reach the new potential density leaf. Equation (4.15) resembles an estimate made by McDougall (1987b) of potential density change along a neutral trajectory [though with $S - \overline{S}$ replaced by $-(\alpha_\theta/\alpha_S)(\theta - \overline{\theta})]$.

Divided by $n^2 g/\alpha$, where n is the local buoyancy frequency, (4.15) gives an estimate of the vertical displacement the float undergoes (positive if upward) in making the transition, namely,

$$z_m - z_{m+1} \cong g\alpha\Delta\Gamma n^{-2}(p_{m+1} - p_m)$$
$$\cong g^{-1}\alpha(\psi - 1)(p_{m+1} - p_m), \quad (4.16)$$

where (2.12) has been used in the first equality and (2.23) in the second. Suppose both sides of (4.16) are divided by Δt, the time taken by the float to move from one central reference pressure, p_m, to the next, p_{m+1}. As $p_{m+1} \rightarrow p_m$ and $\Delta t \rightarrow 0$, the quotient $(p_{m+1} - p_m)/\Delta t$ tends to the rate of change of pressure following horizontal motion along what has been identified as a limiting patched isopycnal, namely σ_N = const, now continuous:

$$(p_{m+1} - p_m)/\Delta t \rightarrow (\partial_t + \mathbf{u} \cdot \nabla_I)p. \quad (4.17)$$

Hence

$$(z_m - z_{m+1})/\Delta t \rightarrow g^{-1}\alpha(\psi - 1)(\partial_t + \mathbf{u} \cdot \nabla_I)p. \quad (4.18)$$

The right side of (4.18) invites comparison to the second term of (2.20), the reversible material flow across orthobaric isopycnals. Thus we see that the material that flows past the hypothetical ballasted float as it travels from one potential

density leaf to the next in the vicinity of a transition pressure is the discrete analogue of the reversible material flow through the corresponding form of orthobaric isopycnal.

e. Regional differentiation

As already noted, Reid's (1994) patching procedure makes allowance for regional variation of T–S properties. That is, different sets of numerical values for the $\sigma_m = \hat{\sigma}(p_m, \sigma_N)$ leaves are selected for one ocean basin compared to another, or for one hemispheric basin compared to the other. For example, Table 1 ⊙ and Figs. 15 ⊙, 16 ⊙ show different patched isopycnal specifications for the North and South Atlantic. Even within a hemispheric basin such as the North Atlantic, Reid (1994) allows for some variation between western and eastern regions (not shown in Table 1 ⊙). This undoubtedly ensures smaller variations of salinity from the regional standard, $S - \overline{S}^R$ (in the mean-square sense, say), than from the lumped global standard salinity $S - \overline{S}^G$. Hence the regional density jumps at transitions, given by (4.15), to which the cross-surface material flow is proportional, is similarly reduced. Likewise the continuously distributed material flow across orthobaric isopycnals could be reduced by using regional averages to define the virtual compressibility rather than lumped global averages as in section 3. However, this reduction comes at a price:there will be horizontal nonconformities in such regionally differentiated patched surfaces (or orthobaric density surfaces) at the boundaries between the regions. Material can leak across these nonconformities just as it does at the vertical transitions between the potential density leaves. It can be shown that the reduction, by using regionally differentiated specifications, of the local material flow across vertical transitions between leaves of a patched surface is compensated by the increase of material exchange at the resulting nonconformities among regions. This is a consequence merely of mass conservation, not of any property of the surfaces.

To illustrate these remarks, an example is shown in Fig. 17 ⊙ of a density section computed for the tropical portion of WOCE Cruise A16 in the Atlantic at 25°W. What is displayed in Fig. 17 ⊙ is σ_4 for each pressure and in situ density pair reported from the station, calculated by bilinear interpolation of the data in Table 1 ⊙. As we have noted, this form of orthobaric density gives a defensible approximation to the patched potential density surfaces of Reid (1994), permitting a continuum of surfaces to be constructed between the standard ones specified. Because different rules are used for calculating σ_4 in the North and South Atlantic (Table 1 ⊙), there are inevitable discontinuities in Fig. 17 ⊙ at the equator, equivalent to vertical displacements of order 50 m. [To forestall possible confusion, we emphasize that σ_4 is not potential density referenced to 4 hbar, but the virtual density of a water parcel taken to 4 hbar *as though* its compressibility were $\Gamma_0 = (\partial\hat{\sigma}/\partial P)_{\sigma_4}$. The latter may be computed by differencing, in effect, Fig. 15 ⊙.] We stress that such discontinuities must occur for patched potential density surfaces interpolated between the surfaces $\sigma_0 = 26.750$ and $\sigma_1 = 31.938$ [these are two of Reid's (1994) standard isopycnals, see Table 1 ⊙; they correspond to $\sigma_4 = 43.837$ and 44.788]. Such discontinuities are a concomitant of the regional differentiation employed in defining the patched potential density surfaces.

These discontinuities constitute gaps through which water may pass, even if the continuous portions of the surfaces could be regarded as material. The necessity of accounting for this exchange of material is a disadvantage of employing regional differentiation of water properties in the definition of patched potential density surfaces. An additional disadvantage of regional differentiation is the forfeiture, in the vicinity of interregional borders, of the property of the Montgomery function of being an acceleration potential (sometimes called a geostrophic streamfunction), as it otherwise is in orthobaric density surfaces, and would be approximately for patched potential density surfaces constructed without regional differentiation (de Szoeke 2000). There are discontinuities in acceleration potential at the interregional borders.

An unexceptionable example of the use of regional differentiation is Reid's (1994) subdivision of the denser waters of the North Atlantic into western and eastern subbasins separated by the Reykjanes Ridge. In this case the differentiated waters are not in direct contact because of the intervening ridge so that no horizontal discontinuity occurs between the differently specified water masses. (A good case could be made for dealing similarly with enclosed marginal seas like the Mediterranean and Red Seas.) Formally this regionality might be specified as follows:

$$\Gamma_0(p, \alpha) = \Gamma_{\text{deep}}(p, \alpha), \qquad\qquad p > p_{\text{max}}$$
$$= \Gamma_A(p, \alpha) \text{ or } \Gamma_B(p, \alpha), \qquad p < p_{\text{max}}, \quad (4.19)$$

depending on whether one is in region A or B (e.g., western or eastern Atlantic).

f. Neutral density

Empirical neutral density variables can be constructed that minimize everywhere the squared difference of the slope of

surfaces of the variable from neutral tangent planes, which are perpendicular to $\nabla\rho - \Gamma_\rho\nabla p$. The calculation may be based on the global hydrographic dataset (Jackett and McDougall 1997), or focused on a single ocean basin like the North Atlantic (Eden and Willebrand 1999). While this idea seems intuitively similar to orthobaric specific volume, which may be thought to be an approximate integral of the left side of Eq. (2.2), an important feature of Jackett and McDougall's (1997) neutral density, which distinguishes it from the universal forms of orthobaric density and patched potential density, is that it depends not only on the thermodynamic state of a water sample, given by the triplet p, T, S but also on the longitude and latitude at which it was observed. (Although regionally differentiated forms of orthobaric density and patched potential density would also possess elements of geographical dependence.) While the complexity of the neutral density algorithm makes it difficult to analyze, we may rely on the empirical demonstration by Jackett and McDougall (1997) that neutral density surfaces closely follow the regionally differentiated form of Reid's (1994) patched potential density surfaces. Indeed, these authors aver that neutral density surfaces are the continuous analogue of discretely defined patched potential density. They presumably mean by this the continuous limit of the discrete spacing of vertical pressure intervals, but also the horizontally continuous analogue of the regionally varying form of the Reid and Lynn (1971) potential density patching method. As we have shown above, both of these procedures (vertical and horizontal patching) imply reversible exchanges of mass across the patches, even if potential density itself could be regarded as perfectly conservative. The continuous limit merely distributes the cross-surface mass exchange at the patches continuously; it does not eliminate it. For orthobaric density surfaces this cross-surface material flow is explicitly given by the second term of Eq. (2.20). For patched potential density surfaces an analogous version of this material flow occurs at the discordances between the segmented leaves of potential density at the transition pressures. For the regionally variable form of patched surfaces, additional horizontal material flows may occur at the borders between the constituent regions, as we saw above. Presumably, for empirical neutral density, cross-surface material flows of both types occur, although now continuously distributed by the Jackett–McDougall algorithm.

5. Summary

An empirically based, pycnotropic (i.e., function only of pressure, $p,$ and in situ specific volume, α), variable was devised. It was constructed by calculating a global fit of adiabatic compressibility to p and α and then using this best-fit compressibility in the density equation to obtain an exact integral of the density tendency and the best-fit compressibility. This exact integral—the desired new variable—may be termed the pressure-corrected or orthobaric specific volume, $v.$ Orthobaric specific volume possesses the same useful dynamical properties potential temperature has in a single-component fluid. First, it possesses a geostrophic streamfunction, the Montgomery function. This means that under circumstances where geostrophy prevails, vertical shear is proportional to the gradient of orthobaric density surfaces (which is the thermal wind relation). Second, to the extent that the tendency of v is negligible, a near-conservative potential vorticity satz may be devised. Neither of these properties pertains for potential density (de Szoeke 2000).

The tendency equation for v was derived. It consists of two parts. One part is given by the same irreversible sources and sinks (including turbulent transport divergence) that contribute to density tendency, multiplied by the buoyancy gain factor ψ, the ratio of apparent stability (proportional to $\partial v/\partial z$) to true stability (buoyancy frequency squared). This factor is quite close to 1, as a diagnostic calculation shows for meridional ocean sections through the Atlantic and Pacific. So this contribution to the orthobaric specific volume tendency $\dot{v}$ is about the same as the potential specific volume tendency $\dot{\alpha}_P$ due to irreversible contributions.

The angle between orthobaric density surfaces and locally defined neutral tangent planes, or trajectories, was calculated for two meridional ocean sections. This angle was sufficiently small that, for the purposes of computing a turbulent diffusivity tensor (assumed to be diagonal with respect to neutral tangent planes) with respect to orthobaric coordinates, it may be neglected except possibly near the ocean bottom.

The other part of the v tendency comes from the compressibility anomaly, the difference between true compressibility and the best-fit compressibility, multiplied by the apparent vertical motion of orthobaric density surfaces. Its magnitude is measured by the smallness of $\psi - 1$, which is proportional to the compressibility anomaly. This term seems to be the inevitable price for banishing salinity gradient contributions from the horizontal momentum balance and hydrostatic balance. Despite the closeness of the gain factor to 1, its contribution to $\dot{v}$ may not be negligible.

For these reasons, we suggest the empirical orthobaric specific volume (or density) variable as an alternative to potential density both for descriptive uses in displaying oceanographic data and for theoretical uses in modeling ocean circulation. It would be premature to claim the "best-fit" compressibility we have devised as the last word. The version based on the global oceanographic data archive suffers from coarse resolution in p and $\alpha.$ The geographical and vertical binning, averaging, and interpolation used in constructing this dataset are not ideal for the present purpose. The partial WOCE station lists available at this time are better for the purpose, but lack extensive geographical coverage. (Still, the concurrence between the NODC archive calculation and the WOCE calculation is encouraging.) The gain factor deserves more careful study. These considerations would lead to a better formulation of best-fit compressibility, and a better assessment of the quasi-conservative quality of orthobaric specific volume.

A remarkable result was established about the method, commonly used in descriptive physical oceanography, of patching locally referenced potential density surfaces from one narrow pressure range to the next (Reid and Lynn 1971). This is that, in the limit of ever narrower pressure ranges over which individual potential density leaves are defined, this method furnishes surfaces that approximate ever more closely surfaces of a form of orthobaric density. (Even without taking the limit, patched potential density surfaces are very similar to a discontinuous form of orthobaric density.) The associations made, in the patching method, among potential density surfaces in adjoining pressure ranges are equivalent to choosing a virtual compressibility function for orthobaric specific volume. From this correspondence between discrete patched potential density and orthobaric density, it follows that accompanying the former there must be cross-surface reversible mass fluxes, quite apart from irreversible mass fluxes associated with mixing and cabbeling, just as there are for orthobaric density. In the case of discrete patched potential density, these reversible fluxes occur at the discontinuous joints between the individual constant potential density leaves. One of the accomplishments of this paper is the determination of the theoretical form of this reversible contribution to the cross-surface mass flux. We also saw that modifications of the patched potential density method, such as varying the matching of potential density surfaces according to geographic regions, correspond to analogous modifications of regionally differentiated orthobaric density surfaces. While these modifications may reduce the reversible cross-surface mass flux locally within a region, this is vitiated by the creation of discontinuities and interlayer mass exchange at the borders between regions.

REFERENCES

Akitomo, K., 1999: Open-ocean deep convection due to thermobaricity. 1. Scaling argument. *J. Geophys. Res.,* **104,** 5225–5234.

Boyer, T., and S. Levitus, 1994: Quality control and processing of historical oceanographic temperature, salinity, and oxygen data. National Oceanic and Atmospheric Administration Tech. Rep. NESDIS 81, U.S. Department of Commerce, 64 pp.

Davis, R. E., 1994: Diapycnal mixing in the ocean: Equations for large-scale budgets. *J. Phys. Oceanogr.,* **24,** 777–800. Find this article online

de Szoeke, R. A., 2000: Equations of motion using thermodynamic coordinates. *J. Phys. Oceanogr.,* **30,** 2814–2829. Find this article online

—— ,and A. F. Bennett, 1993: Microstructure fluxes across density surfaces. *J. Phys. Oceanogr.,* **23,** 2254–2264. Find this article online

Eden, C., and J. Willebrand, 1999: Neutral density revisited. *Deep-Sea Res. II,* **46,** 33–54.

Ekman, V. W., 1934: Review of "Das Bodenwasser und die Gliederung der Atlantischen Tiefsee" by Georg Wüst. *J. Cons. perm. Int. Explor. Mer,* **9,** 102–104.

Ertel, H., 1942: Ein neuer hydrodynamischer Wirbelsatz. *Meteor. Z.,* **59,** 277–281.

Flatté, S. M., Ed., 1979: *Sound Transmission through a Fluctuating Ocean.* Cambridge University Press, 299 pp.

Fofonoff, N. P., 1985: Physical properties of seawater: A new salinity scale and equation of state for seawater. *J. Geophys. Res.,* **90** (C2), 3332–3342.

Jackett, D. R., and T. J. McDougall, 1997: A neutral density variable for the world's oceans. *J. Phys. Oceanogr.,* **27,** 237–263. Find this article online

Lynn, R. J., and J. L. Reid, 1968: Characteristics and circulation of deep and abyssal waters. *Deep-Sea Res.,* **15,** 577–598.

McDougall, T. J., 1987a: Thermobaricity, cabbeling and water mass conversion. *J. Geophys. Res.,* **92,** 5448–5464.

—— ,1987b: Neutral surfaces. *J. Phys. Oceanogr.,* **17,** 1950–1964. Find this article online

—— ,1989: Streamfunctions for the lateral velocity vector in a compressible ocean. *J. Mar. Res.,* **47,** 267–284.

—— ,and C. J. R. Garrett, 1992: Scalar conservation equations in a turbulent ocean. *Deep-Sea Res.,* **39,** 1953–1966.

Montgomery, R. B., 1938: Circulation in upper layers of southern North Atlantic deduced with use of isentropic analysis. *Pap Phys. Oceanogr. Meteor.,* Vol. 6, No. 2, 55 pp.

Phillips, O. M., 1966: *The Dynamics of the Upper Ocean.* Cambridge University Press, 261 pp.

Redi, M. H., 1982: Oceanic isopycnal mixing by coordinate rotation. *J. Phys. Oceanogr.,* **12,** 1154–1158. Find this article online

Reid, J. L., 1994: On the total geostrophic circulation of the North Atlantic Ocean: Flow patterns, tracers and transports. *Progress in Oceanography,* Vol. 33, Pergamon, 1–92.

—— , and R. J. Lynn, 1971: On the influence of the Norwegian–Greenland and Weddell seas upon the bottom waters of the Indian and Pacific oceans. *Deep-Sea Res.,* **18,** 1063–1088.

Sneddon, I. N., 1957: *Elements of Partial Differential Equations.* McGraw-Hill, 327 pp.

Tsuchiya, M., L. D. Talley, and M. S. McCartney, 1992: An eastern Atlantic section from Iceland southward across the equator. *Deep-Sea Res.,* **39,** 1885–1917.

—— , —— , and —— , 1994: Water mass distributions in the western Atlantic: A section from South Georgia Island (54°S) northward across the equator. *J. Mar. Res.,* **52,** 55–81.

Wüst, G., 1933: The stratosphere of the Atlantic ocean. *Scientific Results of the German Atlantic Expedition of the R. V. Meteor 1925–1927,* Vol. 6, Amerind Publishing, 1–107. [Engl. trans. ed. W. J. Emery.].

Tables

Table 1. Specifications of patched isopycnal surfaces.[a]

σ_0	σ_1	σ_2	σ_3	σ_4
		North Atlantic		
26.750	31.090	35.337[d]	39.587[d]	43.837[d]
27.440	**31.938**	36.288[d]	40.538[d]	44.788[d]
27.630	**32.200**	36.550[d]	40.800[d]	45.050[d]
27.824	32.456	**36.980**	41.395	45.735[d]
27.846	32.485	37.017	**41.440**	45.780[d]
27.874	32.523	37.067	**41.500**	45.840[b]
27.892	32.548	37.099	41.539	**45.880**
27.901	32.560	37.115	41.562	**45.907**
27.908	32.569	37.126	41.572	**45.920**
		South Atlantic		
26.750	31.090	35.337[d]	39.587[d]	43.837[d]
27.300	**31.938**	36.288[d]	40.538[d]	44.788[d]
27.630	**32.200**	36.550[d]	40.800[d]	45.050[d]
27.755[c]	32.425	**36.980**	41.400	45.735[d]
27.770	32.445	37.013	**41.440**	45.780[d]
27.787	32.476	37.041	**41.500**	45.840
27.800	32.487	37.057	41.538	**45.880**
27.804	32.498	37.074	41.547	**45.907**
27.815	32.502	37.080	41.564	**45.920**

[a] Excerpted from Reid (1994). Boldface-type numbers indicate Reid's (1994) identification labels for the patched surfaces.
[b] Changed from 45.838.
[c] Corrected (J. L. Reid 2000, personal communication).
[d] Extrapolated.

Click on thumbnail for full-sized image.

Figures
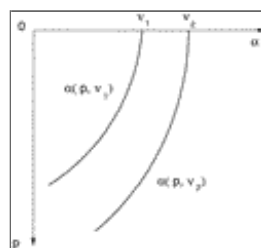
Click on thumbnail for full-sized image.

Fig. 1. Schematic showing a few members of the family $\alpha = \alpha(p, \ v)$, each for fixed orthobaric specific volume v.
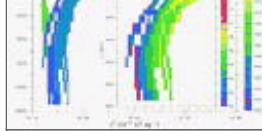
Fig. 2. Average adjusted sound speed c^*_0 (in m s^{-1}) as a function of pressure and adjusted specific volume, α^*, computed from the global $1° \times 1°$ yearly averaged NODC hydrographic dataset
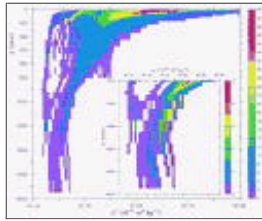
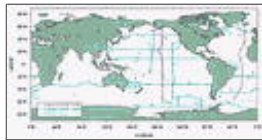Fig. 3. Sound speed standard deviation (in m s^{-1}) about the average shown in Fig. 2
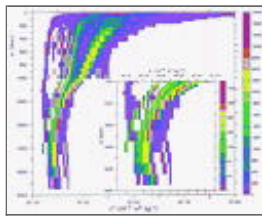
Fig. 4. Number of data points per bin corresponding to the calculations of Figs. 2 and 3

Fig. 5. Data used in the WOCE estimate of average sound speed function $c^*_0(p, \alpha^*)$. The two sections A16 and P16 are displayed in Figs. 8–13
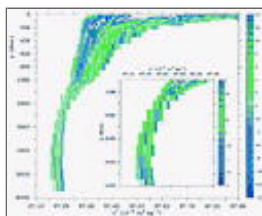
Fig. 6. Difference (in m s^{-1}) between $c^*_0(p, \alpha^*)$ computed from WOCE and NODC (Fig. 2) datasets
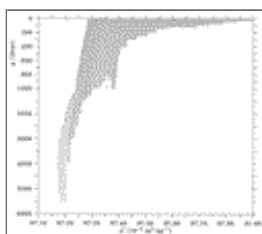
Fig. 7. Isopleths of $v(p, \alpha^*)$ computed by solving Eq. (2.6) using the average sound speed, $c^*_0(p, \alpha^*)$, of Fig. 2
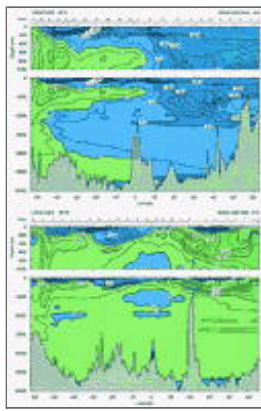
Fig. 8. Sound speed anomaly, $\Delta c = c_0 - c$ (in m s^{-1}), for WOCE sections A16 (top) and P16 (bottom)
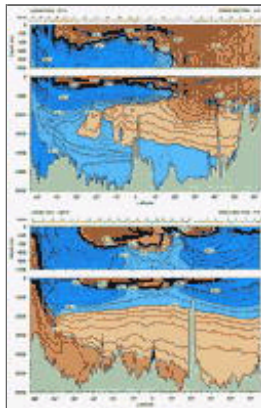
Fig. 9. Salinity, S (in psu), for WOCE sections A16 (top) and P16 (bottom). Different color ranges were used in the two oceans
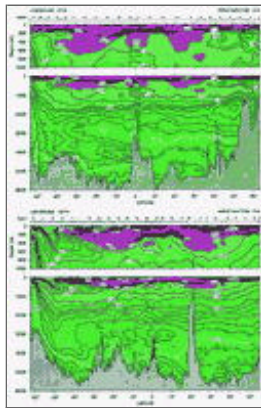
Fig. 10. Buoyancy frequency n, in cycles per hour, for WOCE sections A16 (top) and P16 (bottom). The 0.4 cph contour is shown dashed
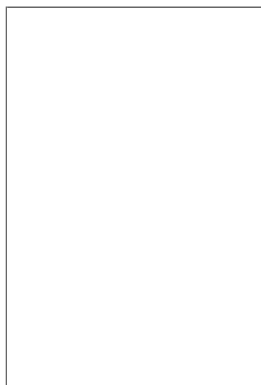
Fig. 11. Gain factor ψ for empirical orthobaric density on WOCE sections A16 (top) and P16 (bottom). The 0.4 cph buoyancy frequency contour from Fig. 10 ⊙ is shown dashed
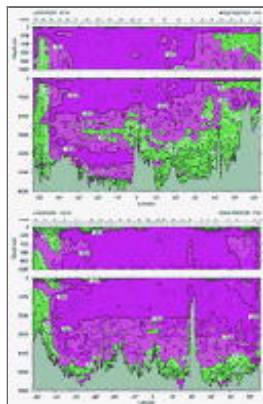
Fig. 12. Logarithm (base 10) of index of neutrality β^2, defined in the text, for empirical orthobaric density on the WOCE sections A16 (top) and P16 (bottom). The 0.4 cph buoyancy frequency contour from Fig. 10 ⊙ is shown dashed
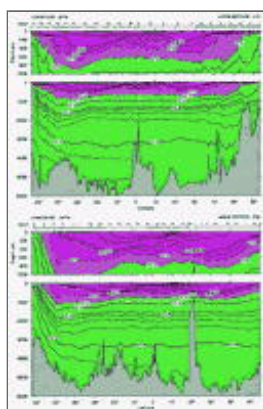
Fig. 13. Empirical orthobaric density σ_v for WOCE sections A16 (top) and P16 (bottom)
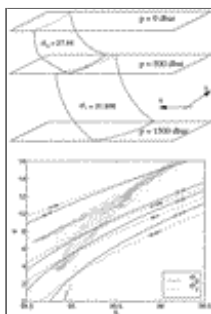
Fig. 14. (a) Patched potential density schematic. A constant σ_0 surface is patched to a σ_1 surface at 500 dbar, and so on, so as to minimize the discordance between the two surfaces or leaves. (b) θ–S diagram for the North Atlantic on 500 dbar (from NODC archive). Pairs of σ_0, σ_1 surfaces were so chosen by Reid (1994) that they intersect in the main θ–S line on this level surface
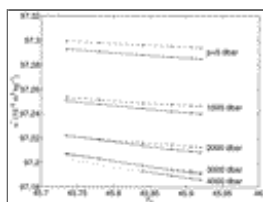
Fig. 15. Orthobaric density function corresponding to Reid's (1994) patched potential density surfaces. Ordinate is in situ density, adjusted by γp [defined in the text]; abscissa is orthobaric density with respect to 4 hbar. Contours at fixed pressure p are shown; South Atlantic (solid), North Atlantic (dashed); pluses indicate the entries from Table 1 ⊙▬
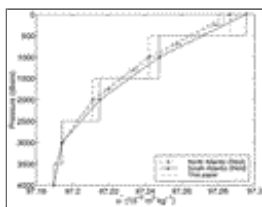
Click on thumbnail for full-sized image.

Fig. 16. Adjusted in situ density vs pressure for orthobaric density $\sigma_4 = 45.88$; stair step and linearly interpolated versions; South Atlantic (solid), North Atlantic (dashed). Asterisks indicate the entries from Table 1 ⊙▬. Orthobaric density based on globally averaged compressibility of section 2 (dot-dashed), with error bars
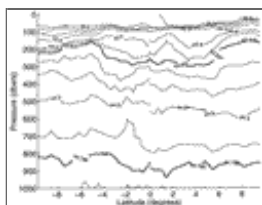
Click on thumbnail for full-sized image.

Fig. 17. Regionally differentiated orthobaric density section for WOCE Cruise A16 along 25°W, based on linear interpolation between Reid's (1994) density surfaces, defined differently for North and South Atlantic. Note the discontinuities at the equator. (Bold isopycnals correspond to the standard Reid surfaces.)

[1] The third variable, salinity, could be replaced by any variable independent of the other two. The ensuing discussion would still follow, with appropriate modifications.

[2] Exact conservation of any such variable is impossible (not only because of irreversible processes). The estimation of the degree of "nearness" to conservation is part of the aim of this paper.

[3] Usually $\alpha\Gamma_\rho$ is called the compressibility. For our purposes, the unconventional usage is convenient.

[4] Although only approximately. The slight dependence of adiabatic lapse rate of seawater on salinity vitiates this useful property.

[5] Reid (1994) shows one additional isopycnal.

[6] The correspondence to the patched density of Reid (1994) can be improved by elaborating the correction γp in Eq. (3.1) to as complicated a function $s(p)$ as necessary to remove as much of the pressure dependence of in situ density as possible in each pressure range. The correction may even be made discontinuous at the transition pressures to optimize this removal.

Corresponding author address: Dr. Roland A. de Szoeke, College of Oceanic and Atmospheric Sciences, Oregon State University, 104 Oceanography Admin. Building, Corvallis, OR 97331-5503.

E-mail: szoeke@oce.orst.edu

top ▲